Anderson Localization from the Berry-Curvature Interchange in Quantum Anomalous Hall Systems

Zhenhua Qiao,[1,2,3] Yulei Han,[1,2] Lei Zhang,[4,5] Ke Wang,[1,2] Xinzhou Deng,[1,2] Hua Jiang,[6,3] Shengyuan A. Yang,[7,3] Jian Wang,[4] and Qian Niu[3,8]

[1]*ICQD, Hefei National Laboratory for Physical Sciences at Microscale, and Synergetic Innovation Center of Quantum Information and Quantum Physics, University of Science and Technology of China, Hefei, Anhui 230026, China*

[2]*CAS Key Laboratory of Strongly-Coupled Quantum Matter Physics, and Department of Physics, University of Science and Technology of China, Hefei, Anhui 230026, China*

[3]*Department of Physics, The University of Texas at Austin, Austin, Texas 78712, USA*

[4]*Department of Physics and the Center of Theoretical and Computational Physics, The University of Hong Kong, Pokfulam Road, Hong Kong, China*

[5]*State Key Laboratory of Quantum Optics and Quantum Optics Devices, Institute of Laser Spectroscopy, and Collaborative Innovation Center of Extreme Optics, Shanxi University, Taiyuan 030006, China*

[6]*College of Physics, Soochow University, Suzhou, Jiangsu 215006, China*

[7]*Research Laboratory for Quantum Materials, Singapore University of Technology and Design, Singapore 487372, Singapore*

[8]*ICQM and CICQM, School of Physics, Peking University, Beijing 100871, China*

(Received 27 January 2016; published 27 July 2016)

We theoretically investigate the localization mechanism of the quantum anomalous Hall effect (QAHE) in the presence of spin-flip disorders. We show that the QAHE stays quantized at weak disorders, then enters a Berry-curvature mediated metallic phase at moderate disorders, and finally goes into the Anderson insulating phase at strong disorders. From the phase diagram, we find that at the charge neutrality point although the QAHE is most robust against disorders, the corresponding metallic phase is much easier to be localized into the Anderson insulating phase due to the *interchange* of Berry curvatures carried, respectively, by the conduction and valence bands. In the end, we provide a phenomenological picture related to the topological charges to better understand the underlying physical origin of the QAHE Anderson localization.

DOI: 10.1103/PhysRevLett.117.056802

Introduction.—Anderson localization [1] is one of the most striking transport phenomena in condensed matter physics. It describes the absence of diffusion of waves due to the severe interference from strong disorders. Based on the scaling theory of localization length, it is known that two-dimensional electrons can be immediately driven into the Anderson insulating phase even in the presence of extremely weak disorders [2]. However, if either the time-reversal symmetry is broken by magnetic field or the spin-rotational symmetry is broken by spin-orbit couplings, a metal-insulator phase transition occurs [3–7], indicating the emergence of a metallic phase at weak disorders.

When the applied magnetic field is strong enough, the resulting Landau-level quantization gives rise to the formation of the conventional quantum Hall effect (QHE) [8,9], manifesting itself as vanishing longitudinal conductance but quantized Hall conductance. In the presence of disorders, there were several different localization mechanisms proposed for the quantum Hall effect, e.g., a levitation theory where extended levels float up to infinity at weak magnetic field limit was used to show that the phase transition can only occur in nearest-neighbor quantum Hall plateaus, indicating that a high QHE state can not directly transit into an insulator [10], while Sheng *et al.* suggested that quantum Hall plateaus are destroyed in a one-by-one order from high to low energies without floating up in energy [11]. When interband mixing effect of opposite chiralities is considered, metallic phase may exist between adjacent quantum Hall plateaus or between the QHE and Anderson insulator [12]. The successful exfoliation of monolayer graphene [13] and realization of $\mathbb{Z}_2$ topological insulators [14,15] (both harbor linear-Dirac dispersions) inspire a broad exploration of the quantum anomalous Hall effect (QAHE) in related materials [16–29] and finally lead to the first realization of the QAHE in magnetically doped topological insulators [30–33], where the QAHE exhibits the same transport properties as those in the conventional QHE. The formation of QAHE usually originates from the synergetic interaction between spin-orbit coupling and intrinsic magnetization. Therefore, a natural and fundamental question arises considering that both the time-reversal and spin-rotational symmetries are broken: How will the QAHE be localized in the presence of strong disorders?

In this Letter, we first investigate the transport properties of the chiral edge states of the QAHE in the presence of both nonmagnetic and spin-flip disorders. In the nonmagnetic case, for Fermi levels lying inside the band gap, the conductance is quantized at weak disorders, gradually decreases at moderate disorders, and finally vanishes at even larger disorders, with the conductance at the charge neutrality point $E_F/t = 0.0$ being always larger than that at any other Fermi level. However, in the spin-flip case, when disorder strength exceeds a critical value, the quantized conductance at $E_F/t = 0.0$ abruptly vanishes, while the conductances at other energies remain finite at even larger disorders. We then show that this anomalous transport phenomenon in a mesoscopic system can be attributed to the interchange of Berry curvatures carried, respectively, by the conduction and valence bands in the corresponding bulk system. Based on the scaling theory of localization length, we provide a phase diagram to show the insulator-metal and metal-insulator phase transitions. At the end, a phenomenological picture is given to understand the physical origin of phase transitions from spin-texture evolutions.

Anomalous edge-state transport.—We start from a prototypical system with a single massive Dirac fermion. Its corresponding tight-binding Hamiltonian in square lattices can be written as [34,35]

$$H = -\frac{iv_F}{2}\sum_i (c_i^\dagger \sigma_x c_{i+\hat{x}} + c_i^\dagger \sigma_y c_{i+\hat{y}} + \text{H.c.}) + \frac{t}{2}\sum_{\langle ij\rangle} c_i^\dagger \sigma_z c_j + \lambda \sum_{\langle i\rangle} c_i^\dagger \sigma_z c_i, \quad (1)$$

where v_F and λ are, respectively, Fermi velocity and mass amplitude. t measures the nearest-neighbor hopping energy. The first term can be considered as a spin-orbit coupling term to form the Dirac dispersion. The second and third terms are, respectively, spin-dependent and constant mass terms, and their competition determines the Chern number of the system. In our consideration, we choose $v_F = t$ and $\lambda = 1.2t$ to realize the QAHE, giving rise to a quantized Hall conductance of $\sigma_{xy} = -e^2/h$. Anderson disorders are included as $H_D = \sum_i w_i^0 c_i^\dagger c_i + w_i^x c_i^\dagger \sigma_x c_i + w_i^y c_i^\dagger \sigma_y c_i$, where the first term is the onsite nonmagnetic disorder, and the last two terms describe spin-flip disorders. $w_{0,x,y}$ are uniformly distributed in an interval of $[-W/2, W/2]$, with W characterizing the disorder strength.

The inset of Fig. 1(a) plots the band structure of a nanoribbon of the QAHE system, where the ribbon width is set to be $N = 80a$ (a is the lattice constant). The gapless edge modes appear inside the bulk gap of $(-0.8t, 0.8t)$ and exhibit a chiral propagating characteristic [39,40], with the red and blue, respectively, indicating the counterpropagating edge modes along opposite boundaries. To explore the disorder effects on the QAHE, we use a two-terminal mesoscopic setup to study the averaged conductance $\langle G\rangle$ as a function of W. The disorders are only added in the central

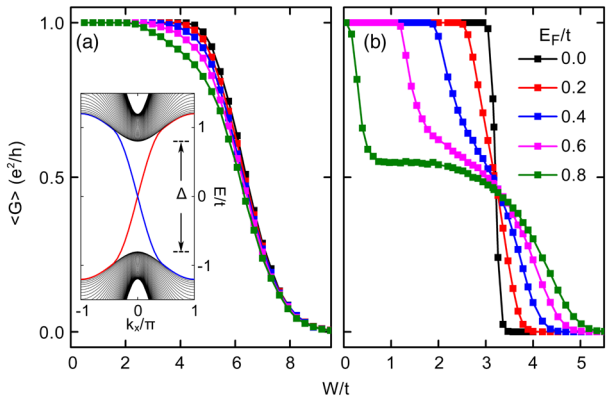

FIG. 1. Averaged conductance $\langle G\rangle$ as a function of W for different Fermi energies inside the bulk gap. The system width is set to be $N = 80a$. (a) and (b) For nonmagnetic and spin-flip disorders, respectively. Over 3000 samples are collected for each point. Inset: Band structure of a nanoribbon displaying the gapless chiral edge states inside the bulk gap Δ.

$N \times N$ scattering region connecting with left and right semi-infinite terminals. Using the Landauer-Büttiker formula [41], the conductance G can be evaluated as

$$G = \frac{e^2}{h}\text{Tr}[\Gamma_L G^r \Gamma_R G^a], \quad (2)$$

where $G^{r,a}$ are, respectively, the retarded and advanced Green's functions of the disordered region, and $\Gamma_{L,R}$ are the line-width functions coupling left and right terminals with the central disordered region.

Since the conduction and valence bands are symmetric about $E_F/t = 0.0$, we choose five representative Fermi energies in our consideration, i.e., $E_F/t = 0.0, 0.2, 0.4, 0.6$, and 0.8. Figure 1(a) displays the averaged conductance as a function of W in the nonmagnetic case. At weak disorders, the conductance keeps quantized at $\langle G\rangle = 1.0e^2/h$. When $W > 2$, all conductances begin to gradually decrease with the increase of W. In particular, the conductance at $E_F/t = 0.0$ is always larger than those at other energies, which is rather reasonable because it requires much more energy to be scattered into the bulk. However, in the spin-flip case, the situation changes completely, with anomalous transport phenomena being observed [see Fig. 1(b)]. For example, at $E_F/t = 0.0$ the conductance keeps quantized until the disorder reaches a critical strength $W_C/t \approx 3.2$, and abruptly vanishes when $W > W_C$. While for other energies, the quantization of the conductance can be destroyed by weak disorders (i.e., the farther away from $E_F/t = 0.0$, the easier to be destroyed). However, the conductance becomes finite in a wide range of disorder strength. In contrast to the nonmagnetic disorder case, at strong disorders $W > W_C$, the closer of the Fermi energy to $E_F/t = 0.0$, the easier of the quantization of conductance to be destroyed. To uncover the fundamental physics that results in these anomalous transport properties, we analyze the Berry curvature density in the corresponding bulk

system that reflects the nature of the anomalous Hall effect [42], and employ the finite-size scaling theory [2] to determine the disorder-induced phase transitions.

Berry curvature analysis.—In our system that features a single gapped Dirac cone at low energy, it is known that the Berry curvature has a peaked distribution about the cone center, contributing to a half-quantized Hall conductance, i.e., $\sigma_{xy} = -\frac{1}{2}\mathrm{sgn}(\lambda)e^2/h$, which is impossible in a noninteracting electronic system. Therefore, the remaining bands must contribute another half-quantized Hall conductance as that from the massive Dirac bands in our considerations [43]. All these are well defined in the absence of disorder, since the Berry curvature from the "massive Dirac bands" is peaked in $\boldsymbol{k}$ space and can be separated from the "remaining bands." However, when disorder is introduced, one can no longer visualize the $\boldsymbol{k}$-space Berry curvature distribution. Instead, we track its distribution in energy by using the disorder averaged Berry curvature and Hall conductance, which can be respectively expressed as [44]

$$\Omega_\alpha = -\sum_{\beta\neq\alpha} \frac{2\mathrm{Im}\langle\alpha|v_x|\beta\rangle\langle\beta|v_y|\alpha\rangle}{(\omega_\beta - \omega_\alpha)^2}, \tag{3}$$

$$\sigma_{xy} = -\frac{e^2}{h}\int d\varepsilon\langle\Omega(\varepsilon)\rangle f(\varepsilon), \tag{4}$$

where $|\alpha\rangle$ indicates the eigenenergy of $|\hbar\omega_\alpha\rangle$ in the disordered system, and $\Omega(\varepsilon) = (1/A)\mathrm{Tr}[\hat{\Omega}\delta(\varepsilon - \hat{H})]$ describes the Berry curvature density in the energy spectrum with $\hat{\Omega}$ being the Berry curvature operator $\hat{\Omega} = \sum_\alpha \Omega_\alpha|\alpha\rangle\langle\alpha|$, and A is the area of the two-dimensional system.

Figure 2 displays the averaged Berry curvature density and Hall conductance as functions of energy E/t for different spin-flip disorder strengths $W/t = 0.0$, 0.2, 1.0, 1.8, 2.6, 3.0, 3.4, and 4.2. At $W/t = 0.0$, although it is impossible to draw a precise separation between the massive Dirac band and the remaining band contributions, by carefully choosing the parameters as used in our consideration we make the two contribution peaks to be separated in either valence or conduction bands [see Fig. 2 (a_1)], which can be generally identified as the contributions from both the massive Dirac bands (labeled as $p_D^{v,c}$) and the remaining bands (labeled as $p_R^{v,c}$), where $v(c)$ denotes valence (conduction) bands and $D(R)$ denotes the Dirac (remaining) bands. For energies inside the gap, $\Omega(E) = 0$, and $\sigma_{xy} = -e^2/h$. When a weak disorder is applied, the bulk gap is nearly unaffected, but the peak $p_D^{v,c}$ from the Dirac bands becomes rather singular [see Fig. 2(a_2)], agreeing with the previous finding reported in Ref. [44]. At moderate disorder strengths as shown in Figs. 2(b)–2(e), one can see that (1) The peaks $p_D^{v,c}$ become slightly broadened and move towards each other between conduction and valence bands in an attractive manner, shrinking the bulk gap, (2) the green and pink colored areas covered by the peaks $p_D^{v,c}$ are approximately constants, corresponding to $\sigma_{xy} \approx \pm 0.5e^2/h$, and (3) the peaks $p_R^{v,c}$ also broaden but move farther away from each other in a repulsive manner. Note that, before the bulk gap closing, the quantized Hall conductance at $E_F = 0$ is most robust against disorders.

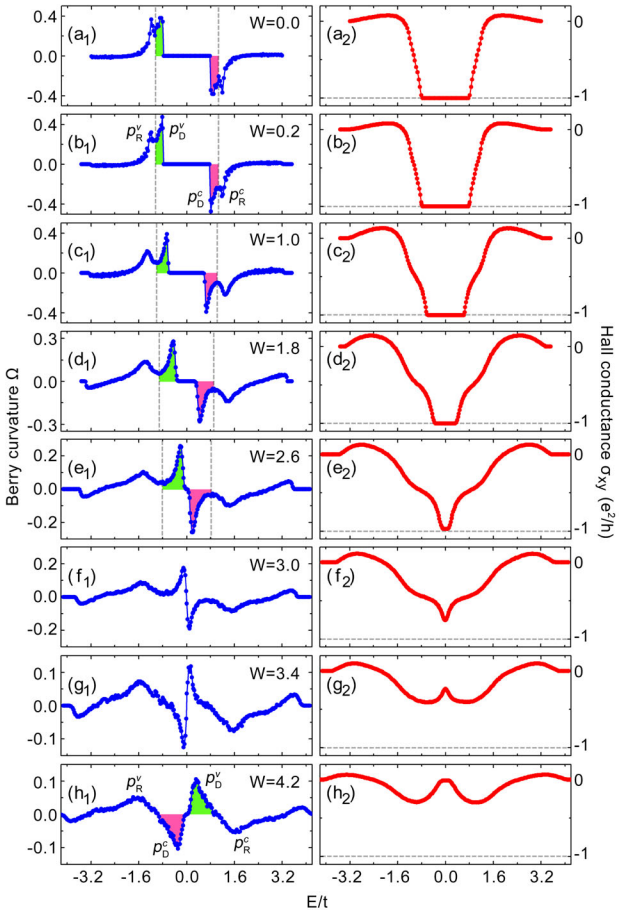

FIG. 2. (a_1)–(h_1): Evolution of averaged Berry curvature density Ω as a function of energy E for different disorder strengths W. The green and pink areas highlight the exchange process of Berry curvatures carried, respectively, by conduction and valence bands. (a_2)–(h_2): Corresponding averaged Hall conductance σ_{xy} as a function of energy E. The supercell is set to be $50a \times 50a$. Over 30 samples are collected for each point.

When the disorder strength approaches a certain critical value, i.e., $W/t \approx 3.0$, the Berry curvatures from both valence and conduction bands become overlapped, closing the bulk gap as displayed in Fig. 2(f). We find that the Hall conductance at $E/t = 0$ suddenly increases, faster than those at other energies. At even stronger disorders, e.g., $W/t = 4.2$, one can see that the two peaks $p_D^{v,c}$ from the conduction and valence bands make an interchange, accompanied with a bulk gap reopening that is also confirmed from the band structure calculation [35]. When the bulk gap is reopened, the Hall conductance becomes exactly zero, i.e., $\sigma_{xy} = 0$. Based on our

integration, the Berry curvatures in the green- or pink-colored regions contribute to a Hall conductance of about $-/+0.5e^2/h$. Therefore, we conclude that it is the interchange of Berry curvatures, carried respectively by the massive Dirac bands from the conduction and valence bands, that leads to the compensation of the Berry curvatures carried by the remaining bands, which is a necessary condition to eliminate the *net* Berry curvature integration below the Fermi level and finally lead to the Anderson localization. By considering various system parameters, we show that it is universal to achieve the anomalous electronic transport and Berry-curvature interchange induced metallic phase for QAHE systems subjected to spin-flip disorders [35]. We believe that the Berry curvature interchange should be closely related to the anomalous transport properties displayed in Fig. 1(b).

Phase transitions.—In order to provide a convincing picture of the phase transitions from the QAHE to Anderson insulator, it is rewarding to employ the finite-size scaling approach to determine the phase boundaries. Based on the well-established transfer-matrix method [45,46], we numerically calculate the localization length ξ on a quasi-one-dimensional bar of essentially infinite length (2×10^6) and finite width L. The periodical condition is applied to eliminate the possible edge-state transport. As an example, in Fig. 3(a) we plot the normalized localization length ξ/L as a function of W/t at $E_F/t = 0.0$ for different widths $L = 32$, 48, 64, and 96. One can find that there are two fixed points, $W_{c1} = 3.18$ and $W_{c2} = 3.23$. At $W < W_{c1}$, ξ/L decreases with the increase of L, indicating that ξ/L will converge to zero when $L \to \infty$, signaling a localized insulating phase, i.e., the QAHE insulating phase. At $W \in [W_{c1}, W_{c2}]$, ξ/L increases with the increase of L, indicating that ξ/L will diverge when $L \to \infty$, signaling a delocalized metallic phase. At $W > W_{c2}$, ξ/L behaves similar to that in the weak disorder case, meaning that it enters a localized insulating phase (Anderson insulator). Therefore, the fixed points W_{c1} and W_{c2} are two critical disorder strengths for the insulator-metal and metal-insulator phase transitions, respectively.

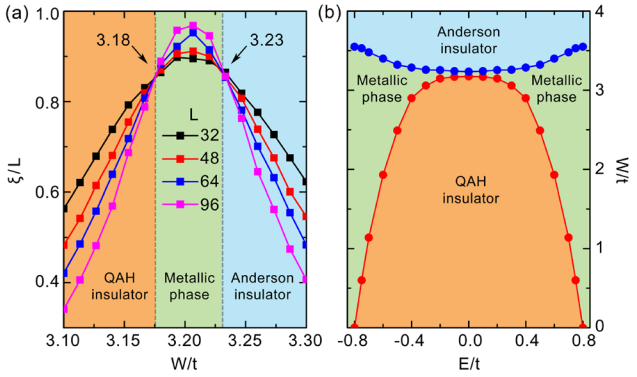

FIG. 3. (a) Normalized localization length ξ/L as a function of the disorder strength W at $E_F = 0.0$ calculated on quasi-one-dimensional bars, with a length of 2×10^6 and different widths of $L = 32$, 48, 64, and 96. $W_{c1} = 3.18$ and $W_{c2} = 3.23$ are two critical points. (b) Phase diagram in (E, W) plane.

After obtaining the two critical disorder strengths W_{c1} and W_{c2} for other representing Fermi energies inside the bulk gap, a phase diagram in the (E, W) plane can be determined [Fig. 3(b)], which is also confirmed from the conductance calculation [35]. At weak disorders, the QAHE phase is robust against disorders, and the charge neutrality point $E_F/t = 0.0$ is most robust. However, at even stronger disorders, it is the charge neutrality point that first enters the Anderson insulating phase from a delocalized metallic phase. This anomalous feature of broadening the metallic phase associated with the Fermi-level shift from $E_F/t = 0.0$ is exactly the fundamental physical origin of the anomalous findings in the above two-terminal conductance calculation [see Fig. 1(b)] and Hall conductance calculation in a finite-sized supercell [see Figs. 2(f_2) and 2(g_2)].

A phenomenological picture.—We now provide a phenomenological picture to better explain the above observed anomalous transport findings and unusual phase diagram. From the topological point of view, the topological order of the quantized Hall conductance can also be described by using the concept of topological charge, which is dependent on the spin textures [47]. In our consideration, the quantized Hall conductance of $\sigma_{xy} = -e^2/h$ is analogous to a Skyrmion, where the valence or conduction bands carry a topological charge of $Q_{v/c} = -/+1$, which can be reflected from the spin-textures as schematically displayed in Fig. 4(a): spins pointing outwards for $Q_c = +1$ (i.e., spins point upwards at the north pole, downwards at the

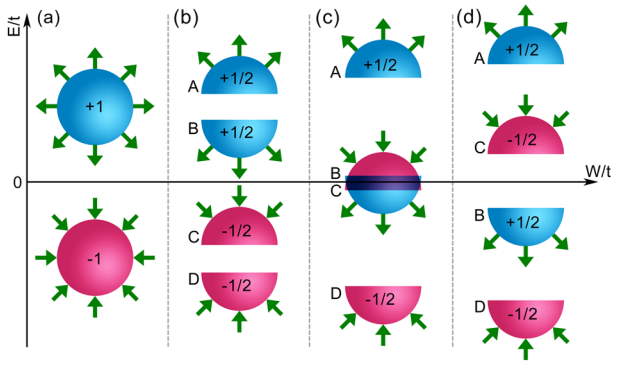

FIG. 4. Schematic of the evolution of topological charges carried by the spin textures (i.e., Skyrmions and merons) of the valence and conduction bands. (a) In the absence of disorders, valence or conduction bands carry a Skyrmion with a topological charge of $Q_v = -1/Q_c = +1$. (b) At weak disorders, the states near the equator of Skyrmions scatter strongly to divide Skyrmions into merons that carry half-integer topological charges and are labeled as "*A*," "*B*," "*C*," and "*D*." (c) By further increasing disorder strength, merons *A* and *D* respectively move upwards and downwards, while merons *B* and *C* move towards each other. (d) At even stronger disorders, merons *B* and *C* make an exchange to cancel out the topological charges in the new valence (conduction) bands by combing merons *A* and *C* (*B* and *D*).

south pole, and in-plane at the equator), but spins pointing inwards for $Q_v = -1$ (i.e., spins point downwards at the north pole, upwards at the south pole, and in-plane at the equator). When the spin-flip disorders are applied, the electronic states near the equator scatter strongly due to the coexistence of different spins, while those at the south and north pole are nearly inactive because of the absence of allowed states with opposite spin. This results in the separation of Skyrmions into merons (labeled as "A", "B", "C" and "D") with $\pm 1/2$ topological charges as labeled in Fig. 4(b). With the increase of disorder strength, merons B and C move towards each other in an attractive manner, while merons A and D move in a repulsive manner as displayed in Fig. 4(c). Note that, at certain disorder strength, merons B and C become spatially overlapped, but no scattering occurs because they are not allowed to scatter between the same spins, which explains the formation of the Berry-curvature mediated metallic phase in Fig. 3. At even larger disorder strength, merons B and C move, respectively, into the valence and conduction bands. At this point, the topological charges carried by the occupied valence bands become zero, leading to the vanishing of Hall conductance and the occurrence of Anderson localization, which can clearly explain the sudden vanishing of the two-terminal conductance and why the charge neutrality point enters the Anderson insulator first. For high-Chern-number QAHE systems, the meron exchange picture would be more complicated and highly depend on the model details [35], which is out of scope of the current work.

Conclusions.—In summary, we theoretically study the disorder effect of the QAHE system in the presence of spin-flip disorders. We show that the system first transitions into a metallic phase from the QAHE insulating phase at moderate disorder strengths, and then further transitions into the Anderson insulating phase. Counterintuitively, we find that it is the charge neutrality point (i.e., $E_F/t = 0$), at which the quantized Hall conductance is most robust against weak disorders but the corresponding metallic phase is easiest to be completely localized into the Anderson insulating phase. By analyzing the Berry curvature evolution, we find that the resulting anomalous electronic transport and Anderson localization at the charge neutrality point originate from the *interchange* of Berry curvatures carried, respectively, by the valence and conduction bands. The finite-size localization length scaling approach is used to determine the phase boundaries separating the three phases: QAHE insulating phase, Berry-curvature mediated metallic phase, and the Anderson insulating phase. In the end, a phenomenological picture from the topological charges is given to explain the anomalous electronic transport and Anderson localization at the charge neutrality point.

We are grateful to D.-N. Sheng, J.-R. Shi, and A. H. MacDonald for valuable discussions. This work was financially supported by the China Government Youth 1000-Plan Talent Program, Fundamental Research Funds for the Central Universities (WK3510000001 and WK2030020027), NNSFC (11474265, 11374219, 11534001, and 91121004) and the National Key R & D Program (2016YFA0301700). Z. Q. also acknowledges support from the U.S. Department of Energy (DE-FG03-02ER45958, Division of Materials Science and Engineering), and the Welch Foundation (F-1255) during his stay at UT Austin. Q. N. acknowledges support from China 973 Program (2013CB921900 and 2012CB921300) during his visit at Peking University. S. A. Y. acknowledges support by Singapore MOE Academic Research Fund Tier 1 (SUTD-T1-2015004). J. W. thanks the University Grant Council (AoE/P-04/08) of the Government of HKSAR for financial support. The Supercomputing Center of USTC is gratefully acknowledged for their high-performance computing assistance.

[1] P. W. Anderson, Phys. Rev. **109**, 1492 (1958).
[2] E. Abrahams, P. W. Anderson, D. C. Licciardello, and T. V. Ramakrishnan, Phys. Rev. Lett. **42**, 673 (1979).
[3] C. W. J. Beenakker, Rev. Mod. Phys. **69**, 731 (1997). And references therein.
[4] M. Onoda, Y. Avishai, and N. Nagaosa, Phys. Rev. Lett. **98**, 076802 (2007).
[5] A. Yamakage, K. Nomura, K. I. Imura, and Y. Kuramoto, J. Phys. Soc. Jpn. **80**, 053703 (2011).
[6] A. Yamakage, K. Nomura, K.-I. Imura, and Y. Kuramoto, Phys. Rev. B **87**, 205141 (2013).
[7] H. Obuse, A. Furusaki, S. Ryu, and C. Mudry, Phys. Rev. B **76**, 075301 (2007).
[8] K. Klitzing, G. Dorda, and M. Pepper, Phys. Rev. Lett. **45**, 494 (1980).
[9] R. B. Laughlin, Phys. Rev. B **23**, 5632 (1981).
[10] S. Kivelson, D.-H. Lee, and S.-C. Zhang, Phys. Rev. B **46**, 2223 (1992).
[11] D. N. Sheng and Z. Y. Weng, Phys. Rev. Lett. **78**, 318 (1997).
[12] G. Xiong, S.-D. Wang, Q. Niu, D.-C. Tian, and X. R. Wang, Phys. Rev. Lett. **87**, 216802 (2001).
[13] A. H. Castro Neto, F. Guinea, N. M. R. Peres, K. S. Novoselov, and A. K. Geim, Rev. Mod. Phys. **81**, 109 (2009).
[14] M. Z. Hasan and C. L. Kane, Rev. Mod. Phys. **82**, 3045 (2010).
[15] X. L. Qi and S.-C. Zhang, Rev. Mod. Phys. **83**, 1057 (2011).
[16] F. D. M. Haldane, Phys. Rev. Lett. **61**, 2015 (1988).
[17] For recent reviews on the quantum anomalous Hall effect, seeH. Weng, R. Yu, X. Hu, X. Dai, and Z. Fang, Adv. Phys. **64**, 227 (2015); C.-X. Liu, S.-C. Zhang, and X.-L. Qi, Annu. Rev. Condens. Matter Phys. **7**, 301 (2016); Y. F. Ren, Z. H. Qiao, and Q. Niu, Rep. Prog. Phys. **79**, 066501 (2016).
[18] M. Onoda and N. Nagaosa, Phys. Rev. Lett. **90**, 206601 (2003).
[19] C. X. Liu, X. L. Qi, X. Dai, Z. Fang, and S. C. Zhang, Phys. Rev. Lett. **101**, 146802 (2008).
[20] C. Wu, Phys. Rev. Lett. **101**, 186807 (2008).
[21] R. Yu, W. Zhang, H. J. Zhang, S. C. Zhang, X. Dai, and Z. Fang, Science **329**, 61 (2010).

[22] Z. H. Qiao, S. A. Yang, W. X. Feng, W.-K. Tse, J. Ding, Y. G. Yao, J. Wang, and Q. Niu, Phys. Rev. B **82**, 161414 (2010).
[23] Z. F. Wang, Z. Liu, and F. Liu, Phys. Rev. Lett. **110**, 196801 (2013).
[24] K. F. Garrity and D. Vanderbilt, Phys. Rev. Lett. **110**, 116802 (2013).
[25] C. Fang, M. J. Gilbert, and B. A. Bernevig, Phys. Rev. Lett. **112**, 046801 (2014).
[26] J. Wang, B. Lian, H. Zhang, Y. Xu, and S.-C. Zhang, Phys. Rev. Lett. **111**, 136801 (2013).
[27] H. Jiang, Z. H. Qiao, H.-W. Liu, and Q. Niu, Phys. Rev. B **85**, 045445 (2012).
[28] H. Pan, Z. Li, C.-C. Liu, G. Zhu, Z. H. Qiao, and Y. G. Yao, Phys. Rev. Lett. **112**, 106802 (2014).
[29] Z. H. Qiao, W. Ren, H. Chen, L. Bellaiche, Z. Y. Zhang, A. H. MacDonald, and Q. Niu, Phys. Rev. Lett. **112**, 116404 (2014).
[30] C. Z. Chang *et al.*, Science **340**, 167 (2013).
[31] J. G. Checkelsky, R. Yoshimi, A. Tsukazaki, K. S. Takahashi, Y. Kozuka, J. Falson, M. Kawasaki, and Y. Tokura, Nat. Phys. **10**, 731 (2014).
[32] X. Kou, S. T. Guo, Y. Fan, L. Pan, M. Lang, Y. Jiang, Q. Shao, T. Nie, K. Murata, J. Tang, Y. Wang, L. He, T.-K. Lee, W.-L. Lee, and K. L. Wang, Phys. Rev. Lett. **113**, 137201 (2014).
[33] C.-Z. Chang, W. Zhao, D. Y. Kim, H. Zhang, B. A. Assaf, D. Heiman, S.-C. Zhang, C. X. Liu, M. H. W. Chan, and J. S. Moodera, Nat. Mater. **14**, 473 (2015).
[34] X.-L. Qi, Y.-S. Wu, and S.-C. Zhang, Phys. Rev. B **74**, 085308 (2006).
[35] See Supplemental Material at http://link.aps.org/supplemental/10.1103/PhysRevLett.117.056802 for additional evidences for the universal finding of the anomalous Anderson localization in quantum anomalous Hall systems, which includes Refs. [36–38].
[36] M. L. Sancho, J. L. Sancho, and J. Rubio, J. Phys. F **14**, 1205 (1984).
[37] D. H. Lee and J. D. Joannopoulos, Phys. Rev. B **23**, 4997 (1981).
[38] S. Sanvito, C. j. Lambert, J. H. Jefferson, and A. M. Bratkovsky, Phys. Rev. B **59**, 11936 (1999).
[39] B. I. Halperin, Phys. Rev. B **25**, 2185 (1982).
[40] A. H. MacDonald and P. Streda, Phys. Rev. B **29**, 1616 (1984).
[41] *Electronic Transport in Mesoscopic Systems*, edited by S. Datta (Cambridge University Press, Cambridge, England, 1995).
[42] D. Xiao, M.-C. Chang, and Q. Niu, Rev. Mod. Phys. **82**, 1959 (2010).
[43] B. A. Bernevig, T. L. Hughes, and S.-C. Zhang, Science **314**, 1757 (2006).
[44] S. A. Yang, Z. Qiao, Y. Yao, J. Shi, and Q. Niu, Europhys. Lett. **95**, 67001 (2011).
[45] A. MacKinnon and B. Kramer, Phys. Rev. Lett. **47**, 1546 (1981); Z. Phys. B **53**, 1 (1983).
[46] L. Sheng, D. Y. Xing, D. N. Sheng, and C. S. Ting, Phys. Rev. B **56**, R7053 (1997); Phys. Rev. Lett. **79**, 1710 (1997).
[47] T. H. R. Skyrme, Nucl. Phys. **31**, 556 (1962); X. Z. Yu, Y. Onose, N. Kanazawa, J. H. Park, J. H. Han, Y. Matsui, N. Nagaosa, and Y. Tokura, Nature (London) **465**, 901 (2010).